Published paper

M. Kovacic, Z. Hanic, S. Stipetic, S. Krishnamurthy and D. Zarko, "Analytical Wideband Model of a Common-Mode Choke," in *IEEE Transactions on Power Electronics*, vol. 27, no. 7, pp. 3173-3185, July 2012.

http://dx.doi.org/10.1109/TPEL.2011.2182060

Analytical Wideband Model of a Common Mode Choke

Marinko Kovacic, Zlatko Hanic, *Student Member,* Stjepan Stipetic, *Student Member,*
Shashank Krishnamurthy, *Member,* Damir Zarko, *Member*

***Abstract*—This paper presents an analytical model of a common mode choke suitable for accurate calculation of the choke impedance over a wide frequency range. The model consists of lumped parameters (resistances, inductances and capacitances) related to individual turns of the coils wound on the core. It takes into account the mutual interactions between the turns and the core with respect to their inductive and capacitive links. The variation of the core permeability and losses with frequency up to 100 MHz is also included. The open-mode impedance characteristic calculated analytically for a VAC 6123x425 single-phase common mode choke shows very good agreement with the 3D finite-element model and the measured characteristic from 150 kHz up to 30 MHz, thus confirming the accuracy of the model over a wide frequency range.**

***Index Terms*—Circuit analysis, Electromagnetic compatibility, Electromagnetic analysis, Inductors, Magnetic cores, Magnetic materials, Permeability, Power filters**

I. Introduction

EVERY power electronic device generates substantial differential-mode (DM) and common mode (CM) noise. An electromagnetic interference (EMI) filter is often required in order to meet the relevant electromagnetic compatibility (EMC) standards. In general, the EMI filter consists of two parts from the functionality standpoint: a DM filter and a CM filter [1]. The common mode choke (CMC) is a part of the CM filter and is used to suppress the line conducted common mode noise that occurs simultaneously on both lines of a conductor pair with respect to a common ground.

The CMC generally consists of a toroidal metallic core with coils wound around the core. The differential mode current (load current) flows through both windings of the CMC in opposite directions and generates two mutually canceling magnetic fields. This current can only be damped by winding ohmic resistance and leakage inductance. On the contrary, the common mode current is damped by the CM impedance. The value of the choke impedance at a certain frequency is a merit of attenuation of the noise signal. The impedance varies with frequency depending on variation of the core permeability and losses with frequency, and on parasitic (stray) capacitances and leakage inductances of the choke coils. Therefore, in order to obtain a wide band analytical model of the common mode choke, it is crucial to accurately calculate the parasitic capacitances and leakage inductances.

Marinko Kovacic, Zlatko Hanic, Stjepan Stipetic and Damir Zarko are with the Department of Electric Machines, Drives and Automation, Faculty of Electrical Engineering and Computing, University of Zagreb, Croatia (e-mail: stjepan.stipetic@fer.hr, marinko.kovacic@fer.hr, zlatko.hanic@fer.hr, damir.zarko@fer.hr). Shashank Krishnamurthy is with the United Technologies Research Center, East Hartford, Connecticut, United States (e-mail: krishnss@utrc.utc.com).

Besides calculation, the impedance characteristic of a CMC can be obtained by measurement. It can be measured in open-mode, common mode and normal (differential) mode. In this paper the experimental data that was available as a reference for comparison with calculated data had been obtained for the case of open-mode impedance in a single-phase choke. Nevertheless, the developed analytical model is also suitable for calculating the common mode and differential mode impedance in either single-phase or three-phase chokes. The open-mode impedance characterizes the impedance of only a single coil in the common mode choke. In a single-phase choke the second coil is open, but there exist both inductive and capacitive links between the two coils of the choke. Any parasitic currents that flow through the turns and capacitive links of an open coil may induce currents in the energized coil as well.

Most of the existing CMC models do not pay attention to individual turns and the geometric structure of the coil. An elementary model of frequency dependent impedance of an inductor on a ferromagnetic core is represented by an equivalent circuit in which the loss free inductance is connected in series with the equivalent loss resistance. This model may be valid up to the first resonant frequency, but a high frequency (HF) model should also include a stray capacitor connected in parallel to the above mentioned series equivalent circuit as stated in [2]–[6].

Mei *et. al* [7] and Jutty *et. al* [8] use a series equivalent circuit which consists of an equivalent inductance and an equivalent loss resistance. The equivalent inductance consists of an ideal inductance and a parallel stray capacitance. Weber *et. al* [9] uses a model of the common mode choke coil which includes a winding stray capacitance connected in parallel to the core loss resistance and to the serial connection of leakage inductance, winding ohmic resistance and coil inductance. Dehong and Xanguo [10] proposed a high frequency lumped parameter model of a common mode inductor. Their model describes the common mode impedance with respect to flux mutual to all the coils, leakage inductance, parasitic capacitance inside the winding and between the windings, and core loss resistance. Dalessandro *et. al* [11] modeled a gapped toroid with the lumped equivalent circuit model that approximates the effects of winding stray capacitances, the winding leakage impedance and the high frequency AC resistance for the frequency range of interest according to [12] and [13]. The core behavior was modeled with the capacitance-

permeance model.

All above mentioned models can in a fairly accurate manner represent the value of the impedance and the slope of the impedance characteristic of an inductor wound on a ferromagnetic core at lower frequencies as well as predict the existence of higher resonant frequencies. However, those models do not include information on lumped parameters related to every single turn, because their lumped parameters represent the entire winding or coil.

Grandi *et. al* [14] proposed a HF equivalent circuit of a single-layer solenoid air-core inductor with a shield. The circuit consists of lumped parameters related to individual turns or pairs of turns of the winding (turn resistance, self-inductance of a turn, mutual inductances between all turns, turn-to-turn capacitances and turn-to-shield capacitances). The HF equivalent circuit was furthermore simplified to present the lumped parameters of the entire inductor winding.

Many papers deal with calculation of self and mutual inductances of single layer solenoid air-core inductors [6], [15], mostly using Grover's formulae [16]. Some authors use complex permeability together with standard formula for inductance of a coil wound on a toroidal ferromagnetic core. The lack of leakage inductance affects the results leading to incorrect values of frequency dependent impedance when compared to measurements [17]. The method for calculating leakage inductance in toroidal ratio transformers was presented in [18].

The problem of calculating the self and mutual inductances for coils on ferromagnetic cores of circular cross-section was thoroughly discussed by Wilcox *et. al.* [19], [20]. These papers establish a set of self and mutual impedance (equivalent core loss included) formulas obtained by means of integral transform techniques. In the case of a toroidal core, the formulas are reduced to convergent series. They follow directly from the solution of Maxwell's equations and therefore offer the ultimate accuracy. Hurley *et. al.* [21] used the same set of formulas, but for calculation of leakage inductance. Nevertheless, those formulas should be modified to be used for calculation of complex mutual impedance between any two turns of inductor's coils. Nave [22] presented a model which enables the designer to predict the leakage inductance in a common mode choke by calculating the inductance of an air core toroid and afterwards including half of the toroidal ferromagnetic core.

The method for calculation of complex mutual impedances presented in this paper uses the value of the self-inductance related to the magnetic flux that completely links all turns through the core and the values of leakage inductance calculated between any two turns in the coils wound on the core. The leakage inductances are obtained using formulas for scalar magnetic potential for the cases of a current in a hollow iron cylinder [23], current outside an iron cylinder [23] and current above an iron plane.

Some problems concerning the calculation of stray capacitances for a single layer winding were discussed in [6] and [24]. Weber *et. al.* [9] presented a method for calculating the parasitic capacitance of a three-phase CMC with multi-layer windings. Massarini *et. al.* [25] and Grandi *et. al.* [14] presented a valuable method for predicting the stray capacitance based on the analytical approach and the physical structure of inductors. The former deals with single layer solenoid air-core inductors while the latter deals with both single and multiple layer coils including the presence of the core or the shield. Hole and Appel [26] presented a method for recursive calculation of the stray capacitance from the high frequency circuit model of a double layer coil with conducting shield and air core. Heldwein et. al. [27] presented a comprehensive physical characterization and modeling of the three-phase common-mode inductors along with the equivalent circuits that are relevant for their design. The paper also deals with magnetic core saturation issues and its effect on equivalent core resistance.

The wideband analytical description of a CMC presented in this paper requires detailed analysis of the choke coil and core parameters. At relatively low frequencies (e.g. 100 kHz) the dominant parameters are coil inductance and resistance. The inductance is mainly dependent on the core permeability which is frequency dependent. The core losses are modeled as an additional coil resistance and are taken into account by introducing the complex permeability of the core. However, at higher frequencies (several MHz) the influence of parasitic capacitances and leakage inductances is significant and must be taken into account. Hence, the reliability of the analytical model strongly depends on the ability to accurately model all the parasitic effects which affect the common mode impedance at all frequencies.

Due to parasitic effects, the equivalent circuit of a CMC coil becomes complicated because it includes inductive and capacitive links between all the turns of the coil and the turns of all other coils wound on the same core. As the number of turns in the choke varies, so does the topology and complexity of the lumped parameter circuit. The impedance of the choke at a certain frequency equals the impedance of the lumped parameter circuit where the circuit parameters are frequency dependent.

The improved methods for calculation of above mentioned parameters required for the wideband analytical model are presented in this paper. Our model is a general equivalent circuit with lumped parameters related to individual turns or pairs of turns for an inductor with multiple windings wound on a toroidal core (single-phase or three-phase CMC). Those lumped parameters are core loss resistance, single turn self-inductance and turn-to-turn mutual inductances (represented through complex mutual impedance), turn-to-turn capacitance and turn-to core capacitance. The model is verified by comparison with 3D finite-element (FE) simulations and measurements.

One of the main advantages of the proposed analytical model is the fact that every lumped parameter is calculated directly from the CMC geometry of each individual turn with material properties taken into account in the wide frequency range. This feature of the model can be effectively utilized for the purpose of optimizing the CMC geometry.

The FE model used in this paper relies on calculation of parasitic partial capacitances (turn-to-turn and turn-to-core) using 3D electrostatic FE solver and the utilization

of those capacitances as lumped parameters in a 3D time-harmonic FE simulation to obtain the frequency dependent CMC impedance. The choke windings are subdivided into single turns. The parameters such as turn self inductance, mutual inductance to other turns and core losses are calculated by finite-element method (FEM) in the same manner as it has been done analytically. The leakage inductance is extracted from the results of the finite-element analysis (FEA) for comparison with analytical results. A very good agreement between parameters calculated using both methods has been shown, thus confirming the accuracy of the analytical calculation of the parasitic capacitance and the leakage inductance of the CMC. The FE approach is not as fast as analytical method, but it is very useful for observing the electromagnetic state of the CMC more accurately even when the geometry is complicated. It can also be used as a referent method in the CMC model development process.

II. Core Material Properties

The properties of the core material are essential for correct modeling of the choke inductance since core permeability can be modeled to take into account the magnetization of the core and the power dissipation due to losses, which both are reflected on the real and imaginary part of the choke impedance.

The most comon materials for the cores of CMCs are nanocrystalline materials, ferrites or amorphous alloys but sometimes laminated iron alloys (nickel, aluminium, cobalt), powdered iron and carbonyl iron are used [28]. Nanocrystalline (e.g. Vitroperm, Finemet) tape-wound cores are widely used in common mode choke applications due to their unique combination of properties. The combination of very thin tapes (20 µm ± 3 µm) and relatively high electrical resistance (1.1-1.2 µΩ m) ensures minimal eddy current losses and outstanding permeability vs. frequency behavior [29]. The CMC cores are usually epoxy coated or placed in the plastic protection box, which is the preferred solution. The minimum coating thickness cannot be guaranteed and therefore additional overlapping wrapping with mylar foil is applied on some cores. Due to surface roughness and thin interlaminar electrical insulation, the active iron cross-section surface is smaller than the physical iron surface resulting in fill (stacking) factor k_{Fe} for all tape-wound cores to be smaller than one.

For high frequency applications it is very important to use complex permeability $\mu^* = \mu' - j\mu''$ for correct modeling of materials. The amplitude and phase of the coil magnetic flux vary in relation to the current which produces that flux as the frequency increases. Even if the wire resistance is neglected, the coil still has complex impedance due to core losses. The complex self-impedance of a single turn can be represented as a serial combination of inductance and resistance

$$\begin{aligned} j\omega L =& j\omega(\mu' - j\mu'')\frac{h_c}{2\pi}\ln\left(\frac{r_{co}}{r_{cin}}\right) \\ =& j\omega L_s + R_s \end{aligned} \tag{1}$$

where h_c is the axial height, r_{co} is the outer radius and r_{cin} is the inner radius of the core as shown in Fig. 10. According to [2], [27] the equivalent serial resistance can be calculated by using the complex permeability for small signal losses or by using the Steinmetz equation for large signal losses. The resistance for large signal calculated by Steinmetz equation is dependent on the inductor current and is typically larger than the one calculated with the complex permeability. For the design of the CM chokes, it is sufficient to calculate the resistance with the complex permeability, since higher currents lead to higher resistances and, thus, higher attenuation of the CM currents.

For modeling purposes it is best to use the manufacturer's measured data for the complex permeability, but that information over broadband frequency range (e.g. 100 kHz - 100 MHz) is rarely available. The data can be also obtained by measuring the impedance of a coil using an impedance analyzer with only few turns carefully wound on a toroidal core to minimize the parasitic parameters (leakage inductance and parasitic capacitance). Some other measurement methods can be also found in literature [30]. The real and imaginary parts of the complex relative permeability can be obtained from the following equations [11]

$$\begin{aligned} \mu'(f) &= \frac{L_s(f)2\pi}{h_c N^2 \ln(\frac{r_{co}}{r_{cin}})}, \\ \mu''(f) &= \frac{R_s(f)}{h_c f N^2 \ln(\frac{r_{co}}{r_{cin}})} \end{aligned} \tag{2}$$

where N is the number of turns of the coil.

III. Calculation of Complex Inductance

According to (1), all inductances are represented as complex numbers with core losses included. It means that mutual inductances which are derived from the self-inductances are also complex numbers. The full inductance matrix (3) can be built by knowing the self-inductance of every turn and the leakage inductance matrix (4).

$$\mathbf{L} = \begin{pmatrix} L_{11} & M_{12} & \cdots & M_{1j} & \cdots & M_{1N} \\ M_{21} & L_{22} & & & & \\ \vdots & & \ddots & & & \\ M_{i1} & & & L_{ii} & & \vdots \\ \vdots & & & & \ddots & \vdots \\ M_{N1} & \cdots & \cdots & \cdots & \cdots & L_{NN} \end{pmatrix} \tag{3}$$

$$\mathbf{L}_\sigma = \begin{pmatrix} 0 & L_{\sigma 12} & \cdots & L_{\sigma 1j} & \cdots & L_{\sigma Nj} \\ L_{\sigma 21} & 0 & & & & \vdots \\ \vdots & & \ddots & & & \vdots \\ L_{\sigma i1} & & & 0 & & \vdots \\ \vdots & & & & \ddots & \vdots \\ L_{\sigma iN} & \cdots & \cdots & \cdots & \cdots & 0 \end{pmatrix} \tag{4}$$

The mutual inductance of turns i and j can be expressed as

$$M_{ij} = L_{ii} - L_{\sigma ij} \tag{5}$$

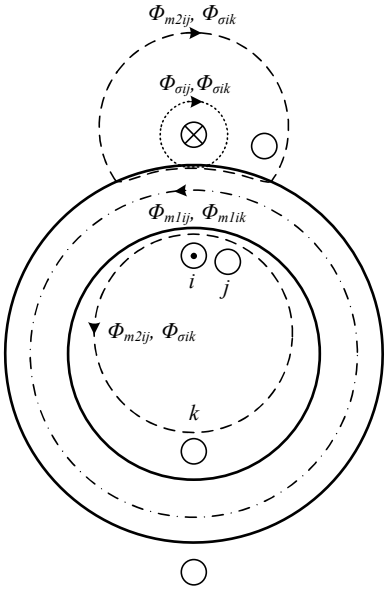

Fig. 1. Magnetic fluxes in the CMC

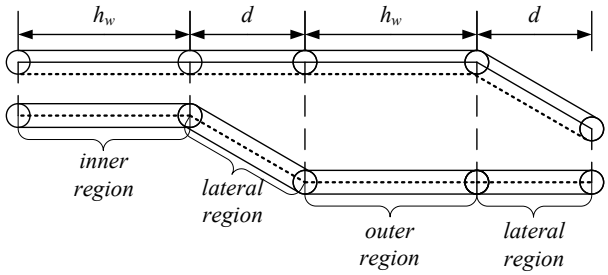

Fig. 2. Two unfolded turns

where L_{ii} is the self-inductance of turn i and $L_{\sigma ij}$ is the leakage inductance of turn i with respect to turn j. The self-inductance L_{ii} consists of two parts (Fig. 1). The first part of the self-inductance, L_{m1}, relates to the magnetic flux that completely links all turns through the core (Φ_{m1ij}, Φ_{m1ik}). The second part of the self-inductance, L_{m2}, relates to the magnetic flux that partially closes through the air and links turns i and j (Φ_{m2ij}). At the same time Φ_{m2ij} is a part of the leakage flux ($\Phi_{\sigma ik}$) for those turns which are not linked by the flux of the i^{th} turn, e.g. k^{th} turn. Therefore in order to include the entire flux of the i^{th} turn, L_{m2} is calculated from its maximum leakage flux. The self-inductance of the i^{th} turn can be expressed as

$$L_{ii} = L_{m1} + L_{m2} = L_{m1} + \max_{j} L_{\sigma ij} \tag{6}$$

The inductance L_{m1} is given by

$$L_{m1} = k_{Fe}\mu^* N^2 \frac{h_c}{2\pi} \ln\left(\frac{r_{co}}{r_{cin}}\right) \tag{7}$$

where k_{Fe} is the core fill factor. The core fill factor is introduced to obtain the effective permeability of the core ($\mu^*_{eff} = k_{Fe}\mu^*$) and take into account the reduced active iron cross-section due to core lamination while retaining the actual outer dimensions of the core (r_{co} and r_{cin}). Since inductances are analyzed on a single turn level, N should be 1. The relative permeability of the core material is assumed to be constant at a certain frequency and equal to the value on the linear part of the B-H characteristic. This assumption is justified if the CMC is designed to maximize the impedance for maximum attenuation of the noise signal. In that case the choke should be designed with unsaturated core. The core permeability is frequency dependent which makes the inductance matrix frequency dependent as well.

The nanocrystalline materials show significant drop of absolute complex permeability at frequencies above a certain frequency. The imaginary part of complex permeability shows a resonant behaviour while the real part shows a relaxation behaviour (Fig. 14). Both effects can be explained with solid state physics (gyromagnetic resonance, resonance relaxation of domain walls) [28], [31]–[33].

The leakage inductance $L_{\sigma ij}$ can be calculated from the analytical field solution and approximations of the field solution. The leakage flux between two turns ($\Phi_{\sigma ij}$, $\Phi_{\sigma ik}$), which is in fact the flux created by current in the energized turn (i) that does not link the other turn (j or k), can be calculated by integrating the magnetic flux density $\mathbf{B}$ over a surface between the two observed turns. The surface between turns can be divided into three regions due to different field solutions: inner, outer and lateral (Fig. 2). The basic dimensions and layout of turns are given in Fig. 3. The crosses and dots mark the referent direction of common mode current in both windings. The field solutions are calculated in the area between the surface of the energized turn and the center of the observed turn. The current in the field solution is placed in the center of the energized turn (dotted lines in Fig. 2 represent limits of integration). The flux inside the energized conductor is also considered and is calculated separately. The field solution for the inner conductor is approximated with a model of a current in a hollow iron cylinder [23] and the field solution for the outer conductor is approximated with a model of a current outside an iron cylinder [23]. The lateral field solution is approximated by a model of a current above an iron plane. These field solutions take into account the core permeability which varies with frequency. Since parts of the leakage flux lines close through the core, the leakage inductances are also frequency dependent. Moreover, the skin effect in the conductor affects its internal inductance which is also part of the leakage inductance between two turns.

1) Inner region: The magnetic field of a conductor located in the inner region can be calculated using the solution for a magnetic scalar potential of an infinitely long conductor embedded in a hollow cylinder made of air surrounded by iron of relative permeability μ_r. If a polar coordinate system is defined according to Fig. 4a, where r_{in} is the radial coordinate of the conductor's center with respect to the main axis of the core and r_{cin} is the radius of the iron boundary, which is the same as the inner radius of the core, the scalar magnetic potential Ω_{in} at the point P inside the air cylinder defined by

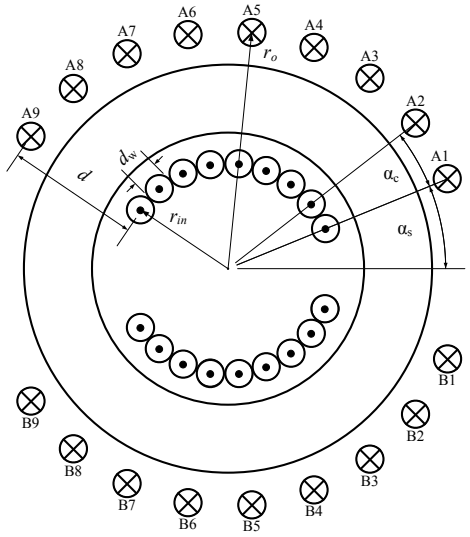

Fig. 3. Layout of turns, basic dimensions and referent directions of common mode current

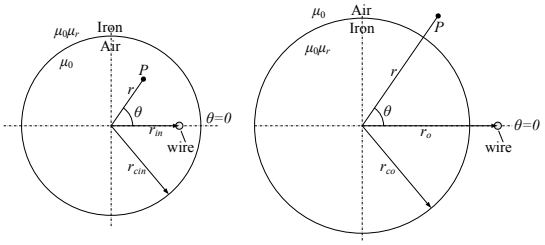

(a) (b)

Fig. 4. (a) Wire embedded in an air cylinder and (b) wire outside an iron cylinder

coordinates r and θ is given by Hague [23]

$$\Omega_{in} = \frac{I}{2\pi}\left[\arctan\left(\frac{r\sin\theta}{r\cos\theta - r_{in}}\right) - \right. \\ \left. - \frac{\mu_r - 1}{\mu_r + 1}\sum_{n=1}^{z}\left(\frac{1}{n}\frac{r^n r_{in}^n}{r_{cin}^{2n}}\sin(n\theta)\right)\right] \tag{8}$$

From the known Ω_{in} one can easily calculate the radial component of the magnetic field $\mathbf{H}$

$$H_{rin} = -\frac{\partial\Omega_{in}}{\partial r} = \frac{I}{2\pi}\left[\frac{r_{in}\sin\theta}{r^2 + r_{in}^2 - 2rr_{in}\cos\theta} + \right. \\ \left. + \frac{\mu_r - 1}{\mu_r + 1}\sum_{n=1}^{\infty}\left(\frac{r^{n-1}r_{in}^n}{r_{cin}^{2n}}\sin(n\theta)\right)\right] \tag{9}$$

where I is the current of the conductor. The differential of surface between two conductors on constant radius r_{in} and with conductor length h_w (Fig. 5) is

$$\mathrm{d}S_{in} = h_w r_{in}\mathrm{d}\theta \tag{10}$$

The conductor length h_w in either inner or outer region has been defined in Section IV in (31).

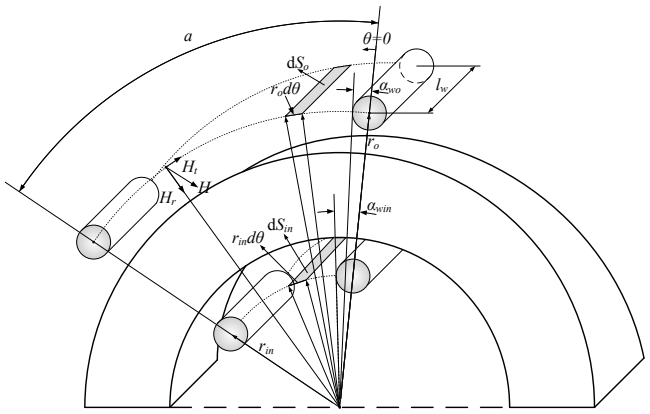

Fig. 5. Integration surface and limits of integration for inner and outer field

The leakage flux is given as

$$\Phi_{\sigma in} = \int_{\theta_{1in}}^{\theta_{2in}} B_{rin}\mathrm{d}S_{in} = \int_{\theta_{1in}}^{\theta_{2in}} \mu_0 H_{rin}\mathrm{d}S_{in} = \\ = \int_{\theta_{1in}}^{\theta_{2in}} \mu_0 H_{rin} h_w r_{in}\mathrm{d}\theta = (\mu_0 h_w r_{in})\int_{\theta_{1in}}^{\theta_{2in}} H_{rin}\mathrm{d}\theta \tag{11}$$

The limits of integration are chosen to include the total leakage flux in the air. Integration starts at the surface of the energized conductor and finishes at the center of the observed conductor. It is the same principle as to integrate the average vector magnetic potential in the observed conductor along the line that goes through the center of the conductor. If α is the angular distance of the centers of two conductors, the limits of the definite integral in (11), according to Fig. 5, are

$$\theta_{1in} = \alpha_{win} = \arcsin\left(\frac{d_w}{2r_{in}}\right) \\ \theta_{2in} = \alpha \tag{12}$$

where d_w is the bare wire diameter.

The internal magnetic field in the energized conductor must be included because the flux inside the energized conductor is also leakage flux in relation to the observed conductor. Due to skin effect the current in the conductor will be concentrated closer to its surface as the frequency increases. The internal inductance of a solid cylindrical conductor with skin effect included will be a function of frequency and can be expressed using either Bessel functions of the first kind with complex argument [34] or the Kelvin functions with real argument [35]. In this particular case the Bessel functions are used since they are easier to calculate using Matlab. The internal inductance for the inner region is then [34]

$$L_{win} = \frac{1}{2\pi f}\mathrm{Imag}\left[\frac{k}{\pi\sigma d_w}\frac{J_0\left(k\frac{d_w}{2}\right)}{J_1\left(k\frac{d_w}{2}\right)}\right]h_w \\ k = \sqrt{2\pi f\mu_c\sigma_c}e^{-\mathrm{j}\frac{\pi}{4}} \tag{13}$$

where J_0 is the complex-valued Bessel function of the first kind of order zero, J_1 is the complex-valued Bessel function of the first kind of order one, σ_c is the conductivity of the conductor, μ_c is the permeability of the conductor (for copper

$\mu_c = \mu_0$), f is the current frequency, j is the imaginary unit and Imag stands for the imaginary part of the expression in the square brackets. The leakage inductance for the inner region between two turns with $r = r_{in}$ is

$$L_{\sigma in} = \frac{\Phi_{\sigma in}}{I} + L_{win} = \frac{\mu_0 h_w}{4\pi} \int_{\alpha_{win}}^{\alpha} \left[\frac{\sin\theta}{1-\cos\theta} + \right. \\ \left. + 2\frac{\mu_r - 1}{\mu_r + 1} \sum_{n=1}^{\infty} \left(\frac{r_{in}}{r_{cin}} \right)^{2n} \sin(n\theta) \right] \mathrm{d}\theta + \\ \frac{1}{2\pi f} \mathrm{Imag} \left[\frac{k}{\pi \sigma d_w} \frac{J_0\left(k\frac{d_w}{2}\right)}{J_1\left(k\frac{d_w}{2}\right)} \right] h_w \tag{14}$$

2) Outer region: The formula for leakage inductance in the outer region between two turns is derived in a similar manner as in the case of inner region, but using formula for scalar potential of an infinitely long conductor outside an iron cylinder of relative permeability μ_r (Fig. 4b) given by [23]

$$\Omega_o = \frac{I}{2\pi} \left[\arctan\left(\frac{r\sin\theta}{r\cos\theta - r_o} \right) + \right. \\ \left. + \frac{\mu_r - 1}{\mu_r + 1} \sum_{n=1}^{z} \left(\frac{1}{n} \frac{r_{co}^{2n}}{r^n r_o^n} \sin(n\theta) \right) \right] \tag{15}$$

where r_o is the radial coordinate of the conductor's center, r_{co} is the radius of the iron boundary, which is the same as the outer radius of the core, and r and θ are the polar coordinates of the point in the air at which the scalar potential is calculated.

The radial magnetic field strength is then

$$H_{ro} = -\frac{\partial \Omega_o}{\partial r} = \frac{I}{2\pi} \left[\frac{r_o \sin\theta}{r^2 + r_o^2 - 2 r r_o \cos\theta} + \right. \\ \left. + \frac{\mu - 1}{\mu + 1} \sum_{n=1}^{\infty} \left(\frac{r_{co}^{2n}}{r^{n+1} r_o^n} \sin(n\theta) \right) \right] \tag{16}$$

In this case the limits of integration (Fig. 5) for calculation of the leakage flux are

$$\theta_{1o} = \alpha_{wo} = \arcsin\left(\frac{d_w}{2r_o} \right) \\ \theta_{2o} = \alpha \tag{17}$$

If the angular distance α between centers of conductors is larger than $\pi/2$, the magnetic flux in the region ($\pi/2$, α) is linked to the second turn due to Ampere's law and large permeability of iron and is no longer leakage flux with respect to the second turn. This is visible from the shape of the leakage flux lines in the outer region as shown in Fig. 1. Therefore, the upper limit of integration in that case is

$$\text{for } \alpha > \frac{\pi}{2};\ \theta_{2o} = \frac{\pi}{2}$$

The leakage flux is calculated in the similar manner as in (11) and therefore the leakage inductance for the outer region between two turns with $r = r_o$ and with internal inductance of the wire included is

$$L_{\sigma o} = \frac{\Phi_{\sigma o}}{I} + L_{wo} = \frac{\mu_0 h_w}{4\pi} \int_{\alpha_{wo}}^{\alpha} \left[\frac{\sin\theta}{1-\cos\theta} + \right. \\ \left. + 2\frac{\mu_r - 1}{\mu_r + 1} \sum_{n=1}^{\infty} \left(\frac{r_{co}}{r_o} \right)^{2n} \sin(n\theta) \right] \mathrm{d}\theta + \\ \frac{1}{2\pi f} \mathrm{Imag} \left[\frac{k}{\pi \sigma d_w} \frac{J_0\left(k\frac{d_w}{2}\right)}{J_1\left(k\frac{d_w}{2}\right)} \right] h_w \tag{18}$$

3) Lateral region: The magnetic field of a current carrying conductor above a permeable plane can be solved using the method of images. The influence of permeable material (magnetization on the boundary) is replaced by introducing another conductor inside the permeable material which is a mirror image. Therefore, the magnetic field **H** has two components at every point: component H_1 due to original current I_1, and component H_2 due to apparent current I_2. The apparent current has the same direction as the original current and can be calculated by

$$I_2 = \frac{\mu - 1}{\mu + 1} I_1 \tag{19}$$

where μ is the permeability of the core. Only the y component of the resultant field (sum of the y components of both fields) passes through surface of integration and is perpendicular to it. The toroidal core is unfolded and all arc lengths between conductor centerlines are preserved. The simple geometry shown in Fig. 6 gives the following relations:

$$H_1 = H_{1y} = \frac{I_1}{2\pi x} \\ H_{2y} = H_2 \sin\beta = \frac{\mu_r - 1}{\mu_r + 1} \frac{I_1}{4\pi h} \cos\beta \sin\beta \tag{20}$$

where h is the distance between the centerline of the conductor and the core surface in the lateral region, and β is the angle between the line which connects the current carrying conductor and its mirror image and the line which connects the centerline of the mirror image and the point at which the field is evaluated (see Fig. 6). According to the same figure for the angle β one can write

$$\tan\beta = \frac{x}{2h} \tag{21}$$

For calculation of the leakage flux between the two conductors in the lateral region the total y component of the field must be calculated which equals $H_y = H_{1y} + H_{2y}$. Therefore combining (20) and (21) yields

$$H_y = \frac{I_1}{2\pi} \left[\frac{1}{x} + \frac{1}{2h} \frac{\mu_r - 1}{\mu_r + 1} \cos\left(\arctan\frac{x}{2h} \right) \sin\left(\arctan\frac{x}{2h} \right) \right] \tag{22}$$

The conductors in the lateral region are not equally spaced along the length, but placed at a constant angle. The leakage flux is then given as a double integral

$$\Phi_{\sigma l} = \mu_0 \int_0^d \int_{d_w/2}^{(z+r_{in})\alpha} H_y \mathrm{d}x \mathrm{d}z \tag{23}$$

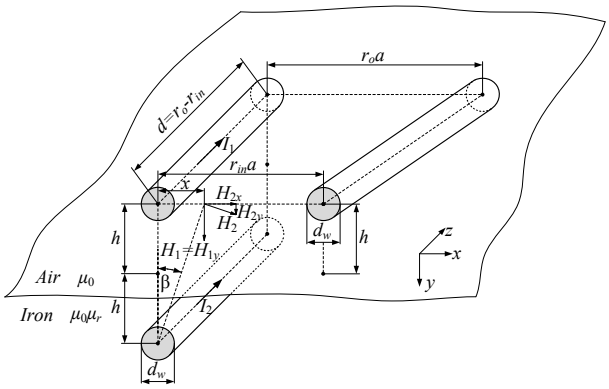

Fig. 6. Integration surface and limits of integration for the lateral field

where $d = r_o - r_{in}$ is the length of the conductor in the lateral region. The leakage inductance in the lateral region with internal inductance of the wire included is then

$$L_{\sigma l} = \frac{\Phi_{\sigma l}}{I_1} + L_{wl} = \mu_0 \int_0^d \int_{d_w/2}^{(z+r_{in})\alpha} H_y \mathrm{d}x\mathrm{d}z + \frac{1}{2\pi f} \mathrm{Imag}\left[\frac{k}{\pi\sigma d_w} \frac{J_0\left(k\frac{d_w}{2}\right)}{J_1\left(k\frac{d_w}{2}\right)}\right] d \tag{24}$$

There are two equal lateral regions and therefore the total leakage inductance between two turns is

$$L_\sigma = L_{\sigma in} + L_{\sigma o} + 2L_{\sigma l} \tag{25}$$

It is easy to find analytical solutions for integrals in (14), (18) and (24) in an explicit form or numerical integration can be used instead.

IV. Calculation of Capacitance

The method for calculation of capacitance considers only single layer CMCs. The method analyzes two types of capacitance: capacitance between two adjacent turns (turn-to-turn) and capacitance between core and turn (turn-to-core). All other capacitances in the model (turn-to-nonadjacent-turn and turn-to-ground) can be neglected since they are at least one order of magnitude smaller. It is assumed that CMC winding turns are equidistant from each other and from the CMC core. Under this assumption all turn-to-turn capacitances will be the same. The same is valid for all turn-to-core capacitances.

According to [6] and [25], the analytical calculation of turn-to-turn and turn-to-core capacitance starts from

$$\mathrm{d}C = \epsilon \frac{\mathrm{d}S}{x} \tag{26}$$

where $\mathrm{d}C$ represents the differential of capacitance between two corresponding surface differentials $\mathrm{d}S$, x is the length of electric field lines between them and ϵ is the permittivity of the material. If an electric field line passes trough layers of material with different permittivity, a modified equation (26) could be used as follows

$$\mathrm{d}C = \epsilon_0 \frac{\mathrm{d}S}{\sum_i \frac{x_i}{\epsilon_{ri}}} \tag{27}$$

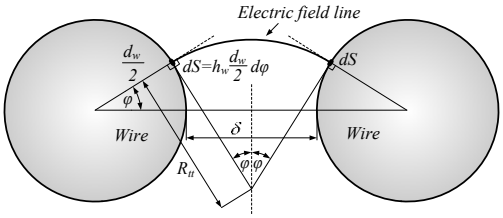

Fig. 7. Geometric configuration used for calculation of turn-to-turn capacitance. For the inner region $R_{tt} = R_{ttin}, \delta = \delta_{in}$ and for the outer region $R_{tt} = R_{tto}, \delta = \delta_o$

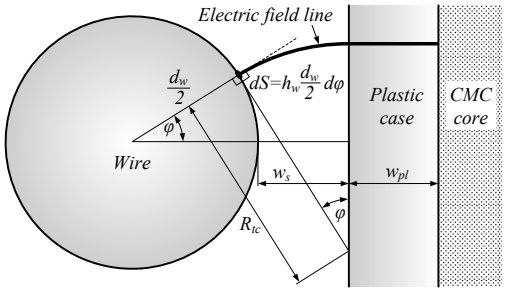

Fig. 8. Geometric configuration used for calculation of turn-to-core capacitance

where ϵ_{ri} is the permittivity of material along the path x_i.

The application of (26) and (27) requires a knowledge of electric field distribution. In [6] and [25] the electric field lines between adjacent turns are approximated with parallel straight lines. It is a good approximation when turns are placed next to each other. This is often not the case for a single layer CMC, especially in the outer region. For calculation of turn-to-turn capacitance it is much better to approximate the electric field lines with circular arcs. The ends of circular arcs are perpendicular to the wire surface as shown in Fig. 7.

The differential of area $\mathrm{d}S$ and the length of the electric field line x can be expressed as a function of angle φ. Due to geometry of the CMC three different regions are analyzed for calculation of turn-to-turn and turn-to-core capacitance: inner, outer and lateral. Fig. 7 is used to derive the expressions for turn-to-turn capacitance for both inner and outer regions. For the inner region, based on the geometry shown in Fig. 7, the radius of the arc of the electric field line R_{ttin} can be expressed as a function of φ

$$R_{ttin} = \left[\frac{\delta_{in}}{2} + \frac{d_w}{2}(1 - \cos\varphi)\right] \frac{1}{\sin\varphi} \tag{28}$$

where δ_{in} is the distance between wire surfaces of adjacent turns in the inner region measured by arc length (Fig. 9), and d_w is the bare wire diameter. In order to simplify the solutions of the turn-to-turn capacitances the arcs δ_{in} and δ_o in Fig. 9 have been replaced by straight lines connecting the centers of the adjacent conductors (marked as δ in Fig. 7), whose length is equal to the lengths of the arcs depending on whether the turn-to-turn capacitance is calculated for the inner or the outer region. Therefore, the length of the arc of the electric field x_{ttin} can be expressed as

$$x_{ttin} = 2\varphi R_{ttin} = \frac{\varphi\left[\delta_{in} + d_w(1 - \cos\varphi)\right]}{\sin\varphi} \tag{29}$$

According to Fig. 7 the differential of area equals $\mathrm{d}S = h_w \frac{d_w}{2} \mathrm{d}\varphi$. The substitution of (29) into (27) gives the expression for the turn-to-turn capacitance for the inner region C_{ttin} as follows:

$$C_{ttin} = \epsilon_0 h_w \frac{d_w}{2} \int\limits_{-\frac{\pi}{2}}^{\frac{\pi}{2}} \frac{\sin\varphi \mathrm{d}\varphi}{\varphi \left[\delta_{in} + d_w \left(1 - \cos\varphi\right)\right]} \tag{30}$$

where

$$h_w = h_{cpl} + 2w_s + d_w \tag{31}$$

is the wire length in either inner or outer region of the core, h_{cpl} is the height of the core with plastic case (or epoxy coating) included which is defined in Fig. 10, and w_s is the distance between wire surface and the core plastic case as shown in Fig. 8. The capacitance of the wire insulation varnish is neglected in the model. It has a fairly large capacity due to its very low thickness (around 15 µm with relative permittivity $\epsilon_r = 3.5$), but it is connected in series with the portion of the turn-to-turn capacitance pertaining to the electric field in the air, which is significantly lower. Similarly, when considering the turn-to-core capacitance, the wire insulation capacitance is connected in series with a capacitance of the plastic case, which also has much lower value due to its thickness of 1.25 mm with $\epsilon_r = 3$.

Analogue to the calculation of the turn-to-turn capacitance for the inner region, the following equation can be derived for the outer region:

$$C_{tto} = \epsilon_0 h_w \frac{d_w}{2} \int\limits_{-\frac{\pi}{2}}^{\frac{\pi}{2}} \frac{\sin\varphi \mathrm{d}\varphi}{\varphi \left[\delta_{o} + d_w \left(1 - \cos\varphi\right)\right]} \tag{32}$$

where δ_o is the distance between wire surfaces of adjacent turns in the outer region measured by arc length (Fig. 9).

The equation for the lateral turn-to-turn capacitance takes into account linear dependence of distance between wire surfaces of adjacent turns δ as a function of radius r

$$\delta(r) = \frac{\delta_o - \delta_{in}}{r_o - r_{in}} \left(r - r_{in}\right) + \delta_{in} \tag{33}$$

where δ_o, δ_{in}, r_o and r_{in} are defined according to Fig. 9. This linear dependence expressed with (33) is substituted into expression for calculation of the inner turn-to-turn capacitance (30) instead of δ_{in} which leads to a double integral. In addition, the surface differential dS of the lateral region is different from the inner or outer region and it equals $\mathrm{d}S = \frac{d_w}{2} \mathrm{d}\varphi \mathrm{d}r$. Therefore, the turn-to-turn capacitance for the lateral region can be calculated using

$$C_{ttl} = \epsilon_0 \frac{d_w}{2} \times \int\limits_{r_{in}}^{r_o} \int\limits_{-\frac{\pi}{2}}^{\frac{\pi}{2}} \frac{\sin\varphi \mathrm{d}\varphi \mathrm{d}r}{\varphi \left[\frac{\delta_o - \delta_{in}}{r_o - r_{in}} \left(r - r_{in}\right) + \delta_{in} + d_w \left(1 - \cos\varphi\right)\right]} \tag{34}$$

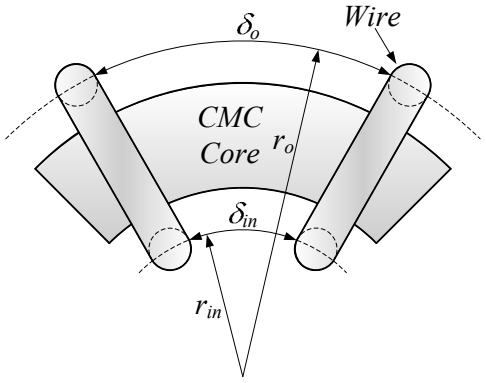

Fig. 9. Geometric configuration of lateral region

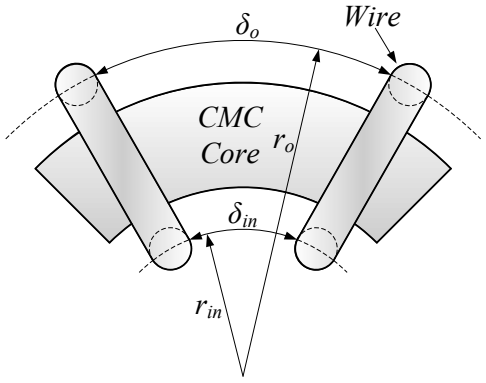

Fig. 10. Definition of parameters for turn-to-core capacitance calculation

Finally, the turn-to-turn capacitance can be calculated as a sum of the inner, outer and lateral turn-to-turn capacitance.

$$C_{tt} = C_{ttin} + C_{tto} + 2C_{ttl} \tag{35}$$

Similarly, for calculation of the turn-to-core capacitance for the inner and outer region the wire length h_w is given by (31). The surface differential $\mathrm{d}S$ can be calculated as $\mathrm{d}S = h_w \frac{d_w}{2} \mathrm{d}\varphi$. Based on the geometric relations shown in Fig. 8, the radius of the arc of the electric field line in the air for the inner region in the case of turn-to-core capacitance can be expressed by

$$R_{tcin} = \left[w_s + \frac{d_w}{2} \left(1 - \cos\varphi\right)\right] \frac{1}{\sin\varphi} \tag{36}$$

The length of the electric field line in the air is therefore

$$x_{tcin} = \varphi R_{tcin} = \frac{\varphi \left[w_s + \frac{d_w}{2} \left(1 - \cos\varphi\right)\right]}{\sin\varphi} \tag{37}$$

The turn-to-core capacitance for the inner region can then be calculated by combining (27), (36) and (37)

$$C_{tcin} = \epsilon_0 h_w \frac{d_w}{2} \int\limits_{-\frac{\pi}{2}}^{\frac{\pi}{2}} \frac{\mathrm{d}\varphi}{\frac{\varphi \left[\delta_c + \frac{d_w}{2} \left(1 - \cos\varphi\right)\right]}{\sin\varphi} + \frac{w_{plin}}{\epsilon_{rpl}}} \tag{38}$$

where w_{plin} is the width of the core plastic case for the inner region (Fig. 10). According to (27) the term $\frac{w_{plin}}{\epsilon_{rpl}}$ represents

the ratio of the length of the electric field line in the plastic case w_{plin} and the relative permittivity of the plastic case ϵ_{rpln}. Similarly, the turn-to-core capacitance for the outer region can be calculated using

$$C_{tco} = \epsilon_0 h_w \frac{d_w}{2} \int_{-\frac{\pi}{2}}^{\frac{\pi}{2}} \frac{\mathrm{d}\varphi}{\frac{\varphi\left[w_s + \frac{d_w}{2}(1-\cos\varphi)\right]}{\sin\varphi} + \frac{w_{plo}}{\epsilon_{rpl}}} \tag{39}$$

where w_{plo} is the width of the core plastic case for the outer region (Fig. 10).

For the lateral region the wire length h_w can be expressed as the difference of r_o and r_{in}. The turn-to-core capacitance for the lateral region is given by

$$C_{tcl} = \epsilon_0 (r_o - r_{in}) \frac{d_w}{2} \times \int_{-\frac{\pi}{2}}^{\frac{\pi}{2}} \frac{\mathrm{d}\varphi}{\frac{\varphi\left[w_s + \frac{d_w}{2}(1-\cos\varphi)\right]}{\sin\varphi} + \frac{w_{pll}}{\epsilon_{rpl}}} \tag{40}$$

where w_{pll} is the width of the core plastic case for the lateral region (Fig. 10).

Finally, the total turn-to-core capacitance can be calculated as a sum of the turn-to-core capacitances in the inner, outer and lateral region.

$$C_{tc} = C_{tcin} + C_{tco} + 2C_{tcl} \tag{41}$$

V. Forming of equivalent circuit and CMC impedance calculation

In this analytical model the CMC windings are subdivided into turns. Each winding in the choke has N turns. Every turn has a complex self-impedance equal to $j\omega L_{ii}$ whose real part, marked as $\bar{R}_{ii}$, represents the core losses and the imaginary part, marked as $\bar{L}_{ii}$, represents the self-inductance of a turn. In addition, every turn has a complex mutual impedance to all other turns equal to $j\omega M_{ij}$, where i and j denote the turn indices. It's real part, marked as $\bar{R}_{ij}$, represents the core losses due to mutual coupling field and the imaginary part, marked as $\bar{M}_{ij}$, represents the mutual inductance between the turns i and j. All turns have turn-to-core capacitance C_{tci}, while the adjacent turns have turn-to-turn capacitance C_{ttij}. Since the last turn in the winding does not have a following adjacent turn, the turn-to-turn capacitance between the first and the second turn in the winding is divided in two equal parts. One half of this turn-to-turn capacitance is connected in parallel to the first turn, and the other half is connected in parallel to the last turn. This is done to achieve better approximation of lumped parameters. The equivalent circuit is shown in Fig. 11.

In order to calculate the impedance of the CMC in open mode, the circuit is supplied by a sinusoidal current source. The ratio of voltage drop on the current source U_s and its current I_s in the phasor domain will give the CMC impedance.

$$Z_{CMC} = \frac{U_s}{I_s} \tag{42}$$

For determination of the voltage drop U_s on the current source, the circuit shown in Fig. 11 must be solved. One can use one of the standard circuit analysis methods (e.g. nodal or mesh analysis method). For obtaining the frequency characteristic of the CMC impedance, the circuit must be solved for every frequency due to frequency dependence of the circuit elements ($\bar{L}_{ii}$, $\bar{R}_{ii}$, $\bar{M}_{ij}$ and $\bar{R}_{ij}$).

An analogue procedure which involves calculation of the complex inductance and capacitance can be used for calculation of the three-phase CMC impedance as well.

VI. Finite-Element Model of the CMC

In order to confirm the results obtained using the analytical model, an FE simulation of the common mode choke has been used. The basic approach is to calculate parasitic capacitances using an electrostatic FE model and afterwards insert them into an electromagnetic time-harmonic FE model as lumped parameters. It is useful to simplify the geometry and significantly shorten the calculation time by using symmetries in the FE model which also have to be satisfied from an electromagnetic point of view. The behavior of the choke can be modeled using only one half of the geometry for capacitance, inductance or impedance calculations. This reduction of model size is visible in the meshed model shown in Fig. 12. The choke cannot be simplified down to one quarter size due to interaction of the second winding and its parasitic capacitance in the high frequency range so one half of the model is the most appropriate to use.

The parasitic capacitance is assumed to remain constant over the entire frequency range so only static FE calculation is required. Only capacitances between two adjacent turns and the core to turn capacitances are taken into account. All other capacitances in the model can be neglected since they are at least one order of magnitude smaller. After calculation of capacitances from the electrostatic FE model, they are inserted as lumped parameters into an electromagnetic time-harmonic FE model. The core material is modeled as solid and non-conductive without laminations since eddy current losses are modeled by frequency dependent complex permeability. The laminated core is modeled by introducing the core fill factor k_{Fe} which reduces the permeability of the core material to take into account the reduced active iron cross-section while retaining the actual outer dimensions of the core. In our particular case $k_{Fe} = 0.8$ which has been determined from the manufacturer's datasheet.

VII. Final results

The analytical model has been tested using a CMC VAC 6123x425 by Vacuumschmelze (Fig. 13a). It is a single layer CMC with nine turns per coil and rather low initial real permeability, i.e. relative real permeability at zero frequency ($\mu_{rinit} = 27000$). The initial real permeability has been determined using (2) and the value of the choke inductance L_s at the frequency of 10 kHz (given in the VAC datasheet as A_L). The complex permeability vs. frequency characteristic for this particular choke shown in Fig. 14 has been obtained by using the known μ_{rinit} combined with cubic interpolation

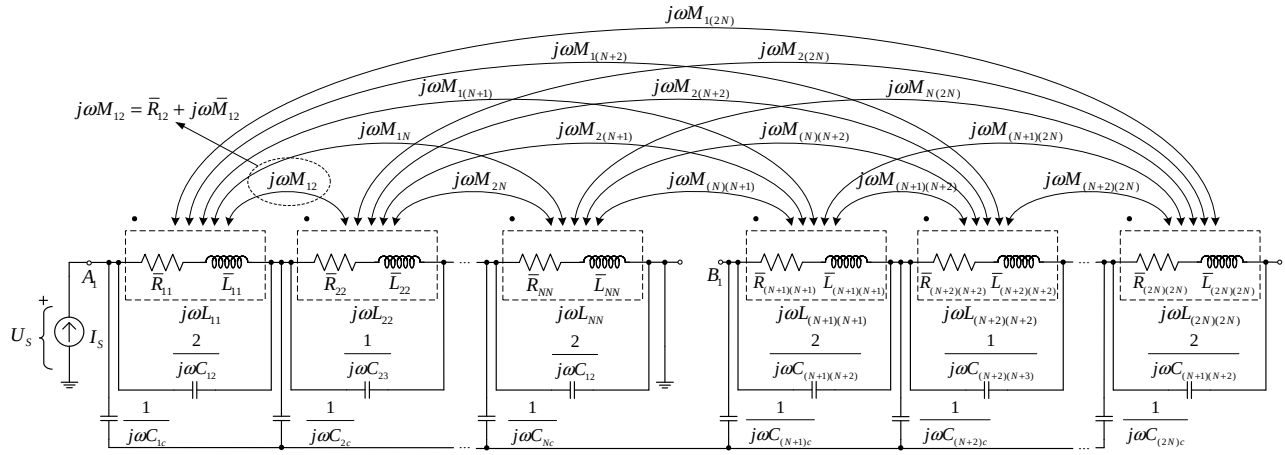

Fig. 11. Equivalent circuit of a single-phase CMC with N turns per coil in open mode

of the manufacturer's data given for the several values of initial permeability. The maximum frequency at which the manufacturer's data for complex permeability was available is 5 MHz. Therefore, the characteristic in Fig. 14 has been extrapolated between 5 MHz and 100 MHz. This characteristic has been used for both analytical and FE models.

The open mode impedance of the choke has been measured using an Agilent 4395A impedance analyzer for the frequency range between 1 kHz and 100 MHz. The manufacturer's datasheets contain only basic geometric data, but detailed data such as number of turns, position of turns, number of layers, overlapping of conductors or winding span have been extracted from the sample choke itself. Although choke coils have not been wound perfectly, for simplicity the analytical model assumes that every elementary turn is the same, the coils are fully symmetrical and all distances between turns and core are constant for all turns. Fig. 15 compares the impedance characteristics for the single-phase VAC 6123x425 choke calculated using analytical model ($Z_{analytical}$), calculated using FEA (Z_{FEA}), obtained from Vacuumschmelze datasheet ($Z_{datasheet}$) and measured using impedance analyzer ($Z_{measured}$). The calculated characteristic show a very good match with characteristics obtained by measurement or from Vacuumschmelze datasheet. There is also an excellent match between analytical and numerical (FE) solutions. The key parameters for high frequency behavior, such as leakage inductance and parasitic capacitances, have been calculated with satisfying accuracy in the analytical model if compared to FE calculation (Tables I and II). The labels of individual turns listed in the tables are shown in Fig. 3. The inductances in Table I are given at zero frequency because calculation of the inductance matrix using Infolytica MagNet software is only possible at zero frequency and with core permeability defined as the real number.

The analytical and FE models have also been compared for the case of a three-phase CMC. Since no actual choke was available for experimental validation, an FE model has been used as a reference instead. The initial permeability of the VITROPERM core material has been set to $\mu_{rinit} = 50000$. The core dimensions have been altered to accommodate three

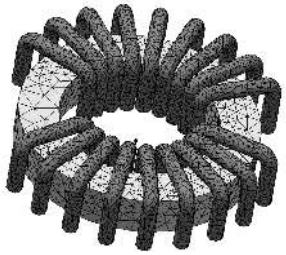

Fig. 12. Mesh generated in Infolytica MagNet for VAC 6123x425 CMC

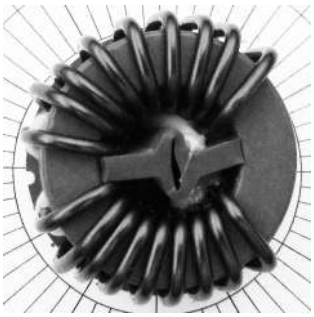

Fig. 13. Photo of the VAC 6123x425 CMC

coils on the core. The outer diameter has been increased from 32.8 mm in the VAC 6123x425 CMC to 42.8 mm. The frequency characteristics of open mode impedance calculated analytically and numerically are compared in Fig. 16b. The analytical model matches well with the FE model in this case as well.

VIII. Conclusion

An analytical model for calculation of common mode choke impedance over a wide frequency range with lumped parameters related to individual turns of the coils wound on the toroidal core has been developed. The model takes into account parasitic capacitances (turn-to-turn and turn-to-core), leakage inductances (for all combinations of turns) and core material properties (frequency dependent permeability). The model represents all inductances of the coil turns (self and

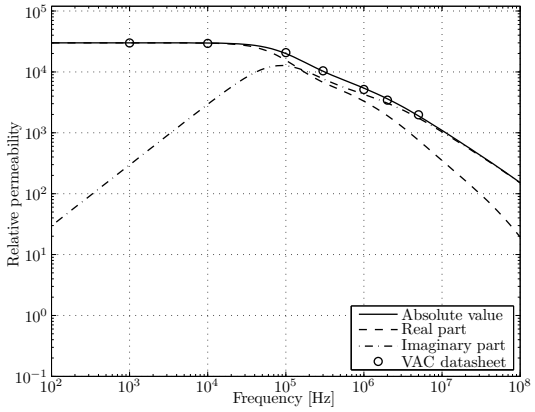

Fig. 14. Complex permeability of the VACx425 nanocrystalline core in the frequency range 100 Hz to 100 MHz for initial relative permeability $\mu_{init} = 27000$

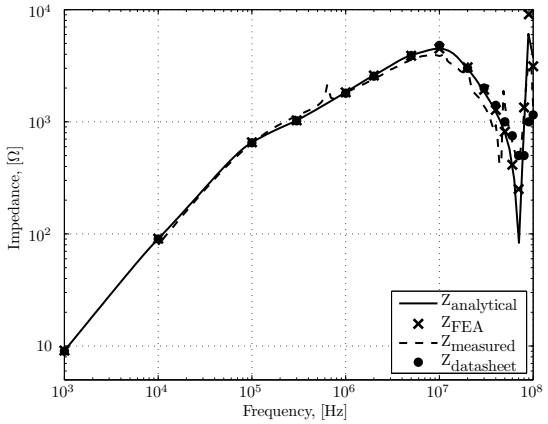

Fig. 15. Comparison of measured, analytically and numerically calculated open mode impedance for VAC 6123x425 CMC

TABLE I
COMPARISON OF LEAKAGE INDUCTANCES BETWEEN TWO TURNS CALCULATED ANALYTICALLY AND BY FEA FOR VAC 6123X425 AT ZERO FREQUENCY

turn pairs	$L_{\sigma AN}$[nH]	$L_{\sigma FEA}$[nH]
A1-A3	26.0	25.5
A1-A4	32.9	32.2
A1-A5	38.1	37.1
A1-A6	42.1	40.9
A1-A7	45.1	43.9
A1-A8	47.4	46.3
A1-A9	49.1	48.3
A1-B1	32.4	31.6
A1-B2	37.7	36.6
A1-B3	41.8	40.5
A1-B4	44.9	43.6
A1-B5	47.2	46.1
A1-B6	49.0	48.1
A1-B7	50.3	49.7
A1-B8	51.1	51.0
A1-B9	51.6	52.0

TABLE II
COMPARISON OF TURN-TO-TURN AND TURN-TO-CORE CAPACITANCES CALCULATED ANALYTICALLY AND BY FEA FOR VAC 6123X425

turn pairs	$C_{tt\,AN}$ [pF]	C_{ttFEA} [pF]	turns	$C_{tc\,AN}$ [pF]	C_{tcFEA} [pF]
A1-A2	1.65	1.47	A1	1.76	1.83
A2-A3		1.46	A2		1.46
A3-A4		1.46	A3		1.46
A4-A5		1.50	A4		1.43
A5-A6		1.50	A5		1.47
A6-A7		1.51	A6		1.48
A7-A8		1.45	A7		1.46
A8-A9		1.55	A8		1.47
B1-B2		1.54	A9		1.76
B2-B3		1.54	B1		1.81
B3-B4		1.43	B2		1.47
B4-B5		1.50	B3		1.47
B5-B6		1.65	B4		1.47
B6-B7		1.55	B5		1.45
B7-B8		1.57	B6		1.44
B8-B9		1.54	B7		1.49
			B8		1.47
			B9		1.78

(a)

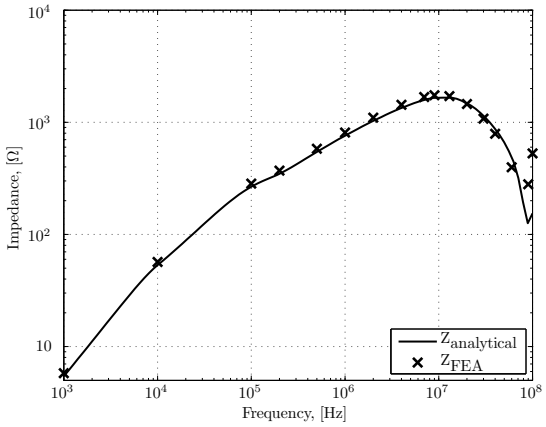

(b)

Fig. 16. 3D FE model (a) and open mode impedance (b) of a three-phase CMC

mutual) as complex numbers thus taking into account the core losses by means of complex permeability.

The equivalent circuit used in the model to represent the choke impedance contains complex self-impedances of individual turns, all combinations of mutual complex impedances between the turns, and parasitic capacitances with respect to adjacent turns and the core. In the case of open mode impedance such topology allows one to calculate the influence of the parasitic currents induced in the open coil on the impedance of the energized coil. Such equivalent circuit is also universally applicable for calculation of the common mode impedance of single-phase and three-phase common mode chokes.

The principal disadvantage of this model is the necessity to provide accurate data for the complex permeability of the core in the frequency range of interest, which is 100 MHz in this particular case. The manufacturers usually provide information about complex permeability up to 10 MHz. If it is desired to calculate the choke impedance up to 100 MHz, then one has to rely on extrapolated data for the complex permeability in which case the accuracy of the model is difficult to predict. It can only be confirmed by measurement of impedance of an actual choke.

The practical problem that emerges when chokes are installed in an actual power electronic device is the appearance of additional parasitic capacitances between the choke winding and the sorrounding grounded elements of the device (e.g. metal case). The model does not take into account those influences.

A comparison is made between open mode impedance characteristic of the VAC 6123x425 single-phase common mode choke calculated using the presented analytical model, calculated using the 3D FE model, obtained from the manufacturer's datasheet and measured using the impedance analyzer. Both calculated impedance characteristics show a good match with the measured one. Moreover, the analytical and the FE model have been also compared for the case of a generic three phase choke with larger outer core diameter and higher initial permeability of the core material with respect to VAC 6123x425. Both models show an excellent match of analytically and numerically calculated impedance characteristics. The accuracy of the analytical model with respect to the referent FE model has also been confirmed in terms of values of parasitic capacitances and leakage inductances for individual turns.

ACKNOWLEDGMENT

This research has been supported by Power Electronics Group, United Technologies Research Center Ltd.

REFERENCES

[1] R. Lai, Y. Maillet, F. Wang, S. Wang, R. Burgos, and D. Boroyevich, "An Integrated EMI Choke for Differential-Mode and Common-Mode Noise Suppression," *Power Electronics, IEEE Transactions on*, vol. 25, no. 3, pp. 539–544, 2010.

[2] M. Bartoli, A. Reatti, and M. Kazimierczuk, "Modelling iron-powder inductors at high frequencies," in *Industry Applications Society Annual Meeting, 1994., Conference Record of the 1994 IEEE*, oct 1994, pp. 1225 –1232 vol.2.

[3] Q. Yu, T. Holmes, and K. Naishadham, "Rf equivalent circuit modeling of ferrite-core inductors and characterization of core materials," *Electromagnetic Compatibility, IEEE Transactions on*, vol. 44, no. 1, pp. 258 –262, feb 2002.

[4] K. V. Schuylenbergh and R. Puers, *Inductive Powering: Basic Theory and Application to Biomedical Systems*. Springer, Jul. 2009.

[5] M. Bartoli, A. Reatti, and M. Kazimierczuk, "High-frequency models of ferrite core inductors," in *Industrial Electronics, Control and Instrumentation, 1994. IECON '94., 20th International Conference on*, vol. 3, sep 1994, pp. 1670 –1675 vol.3.

[6] A. Massarini, M. Kazimierczuk, and G. Grandi, "Lumped parameter models for single-and multiple-layer inductors," in *Power Electronics Specialists Conference, 1996. PESC'96 Record., 27th Annual IEEE*, vol. 1. IEEE, 2002, pp. 295–301.

[7] C. Mei, J. Balda, W. Waite, and K. Carr, "Analyzing common-mode chokes for induction motor drives," in *Power Electronics Specialists Conference, 2002. pesc 02. 2002 IEEE 33rd Annual*, vol. 3. IEEE, 2002, pp. 1557–1562.

[8] M. Jutty, V. Swaminathan, and M. Kazimierczuk, "Frequency characteristics of ferrite core inductors," in *Electrical Electronics Insulation Conference and Electrical Manufacturing & Coil Winding Conference, 1993. Proceedings., Chicago'93 EEIC/ICWA Exposition*. IEEE, 2002, pp. 369–372.

[9] S. Weber, M. Schinkel, S. Guttowski, W. John, and H. Reichl, "Calculating Parasitic Capacitance of Three-Phase Common-Mode Chokes," *Power Conversion Intelligent Motion (PCIM)*, pp. 1–6.

[10] L. Dehong and J. Xanguo, "High frequency model of common mode inductor for emi analysis based on measurements," in *Electromagnetic Compatibility, 2002 3rd International Symposium on*, May 2002, pp. 462 – 465.

[11] L. Dalessandro, W. Odendaal, and J. Kolar, "Hf characterization and nonlinear modeling of a gapped toroidal magnetic structure," *Power Electronics, IEEE Transactions on*, vol. 21, no. 5, pp. 1167 –1175, 2006.

[12] A. Schellmanns, K. Berrouche, and J.-P. Keradec, "Multiwinding transformers: a successive refinement method to characterize a general equivalent circuit," *Instrumentation and Measurement, IEEE Transactions on*, vol. 47, no. 5, pp. 1316 –1321, oct 1998.

[13] A. Schellmanns, P. Fouassier, J.-P. Keradec, and J.-L. Schanen, "Equivalent circuits for transformers based on one-dimensional propagation: accounting for multilayer structure of windings and ferrite losses," *Magnetics, IEEE Transactions on*, vol. 36, no. 5, pp. 3778 –3784, sep 2000.

[14] G. Grandi, M. Kazimierczuk, A. Massarini, and U. Reggiani, "Stray capacitances of single-layer solenoid air-core inductors," *Industry Applications, IEEE Transactions on*, vol. 35, no. 5, pp. 1162–1168, 1999.

[15] G. Grandi, U. Reggiani, M. Kazimierczuk, and A. Massarini, "Optimal design of single-layer solenoid pair-core inductors for high frequency applications," in *Circuits and Systems, 1997. Proceedings of the 40th Midwest Symposium on*, vol. 1. IEEE, 2002, pp. 358–361.

[16] F. W. Grover, *Inductance Calculations: Working Formulas and Tables*. Instrumentation Systems &, Jun. 1982.

[17] S. Weber, M. Schinkel, E. Hoene, S. Guttowski, W. John, and H. Reichl, "Radio Frequency Characteristics of High Power Common-Mode Chokes," in *IEEE Int. Zurich Symp. on Electromagnetic Compatibility*, 2005, pp. 1–4.

[18] A. Binnie and T. Foord, "Leakage Inductance and Interwinding Capacitance in Toroidal Ratio Transformers," *Instrumentation and Measurement, IEEE Transactions on*, vol. 16, no. 4, pp. 307–314, 1967.

[19] D. Wilcox, W. Hurley, and M. Conlon, "Calculation of self and mutual impedances between sections of transformer windings," *Generation, Transmission and Distribution [see also IEE Proceedings-Generation, Transmission and Distribution], IEE Proceedings*, vol. 136, no. 5, pp. 308–314, 2002.

[20] D. Wilcox, M. Conlon, and W. Hurley, "Calculation of self and mutual impedances for coils on ferromagnetic cores," *Physical Science, Measurement and Instrumentation, Management and Education-Reviews, IEE Proceedings A*, vol. 135, no. 7, pp. 470–476, 2008.

[21] W. Hurley and D. Wilcox, "Calculation of leakage inductance in transformer windings," *Power Electronics, IEEE Transactions on*, vol. 9, no. 1, pp. 121–126, 2002.

[22] M. Nave, "On modeling the common mode inductor," in *Electromagnetic Compatibility, 1991. Symposium Record., IEEE 1991 International Symposium on*. IEEE, 1991, pp. 452–457.

[23] B. Hague, *The principles of electromagnetism applied to electrical machines*. Dover Publications, New York, 1962.

[24] Y. Chen, H. Liu, and H. Kong, "The mechanism of turn-to-turn capacitance in inductance winding and its calculation methods," in *Power*

System Technology, 2002. Proceedings. PowerCon 2002. International Conference on, vol. 4. IEEE, 2002, pp. 2173–2178.
[25] A. Massarini and M. Kazimierczuk, "Self-capacitance of inductors," *Power Electronics, IEEE Transactions on*, vol. 12, no. 4, pp. 671–676, 2002.
[26] M. Hole and L. Appel, "Stray capacitance of a two-layer air-cored inductor," in *Circuits, Devices and Systems, IEE Proceedings-*. IET, 2005, pp. 565–572.
[27] M. Heldwein, L. Dalessandro, and J. Kolar, "The three-phase common-mode inductor: Modeling and design issues," *Industrial Electronics, IEEE Transactions on*, vol. 58, no. 8, pp. 3264 –3274, aug. 2011.
[28] A. V. d. Bossche and V. C. Valchev, *Inductors and Transformers for Power Electronics*, 1st ed. CRC Press, Mar. 2005.
[29] J. Petzold, "Advantages of softmagnetic nanocrystalline materials for modern electronic applications," *Journal of Magnetism and Magnetic Materials*, vol. 242, pp. 84–89, 2002.
[30] R. Dosoudil and V. Olah, "Measurement of complex permeability in the RF band," *Journal of Electrical Engineering*, vol. 45, no. 107s, pp. 97–100, 2004.
[31] M. Rosales and R. Montiel, H.and Valenzuela, "Magnetic permeability and relaxation frequency in high frequency magnetic materials," *Mat. Res. Soc. Symp. Proc. Vol. 674*, 2001.
[32] G. Dionne, "Magnetic relaxation and anisotropy effects on high-frequency permeability," *Magnetics, IEEE Transactions on*, vol. 39, no. 5, pp. 3121 – 3126, sept. 2003.
[33] R. Lebourgeois, S. Bérenguer, C. Ramiarinjaona, and T. Waeckerlé, "Analysis of the initial complex permeability versus frequency of soft nanocrystalline ribbons and derived composites," *Journal of Magnetism and Magnetic Materials*, vol. 254, pp. 191–194, 2003.
[34] V. Boras, S. Vujević, and D. Lovrić, "Definition and computation of cylindrical conductor internal impedance for large parameters," in *ICECom, 2010 Conference Proceedings, Dubrovnik, Croatia*, 20–23 Sept. 2010, pp. 1–4.
[35] W. Stevenson, *Elements of Power System Analysis*. McGraw-Hill, New York, 1955.

Marinko Kovacic was born in Split, Croatia on June 2, 1985. He received Dipl. Eng. degree in electrical engineering from the University of Zagreb, Croatia in 2009. Currently he is a Ph.D. student working as a junior researcher at the Department of Electric Machines, Drives and Automation, Faculty of Electrical Engineering and Computing, University of Zagreb.

Zlatko Hanic was born in Zagreb, Croatia on April 14, 1986. He received Dipl. Eng. degree in electrical engineering from the University of Zagreb, Croatia in 2009. Currently he is a Ph.D. student working as a junior researcher at the Department of Electric Machines, Drives and Automation, Faculty of Electrical Engineering and Computing, University of Zagreb.

Stjepan Stipetic was born in Ogulin, Croatia on February 2, 1985. He received Dipl. Eng. degree in electrical engineering from the University of Zagreb, Croatia in 2008. Currently he is a Ph.D. student working as a junior researcher at the Department of Electric Machines, Drives and Automation, Faculty of Electrical Engineering and Computing, University of Zagreb. He is a member of IEEE and the Croatian National Committee of CIGRE. His areas of interest include design, modelling, analysis and optimization of electrical machines.

Shashank Krishnamurthy was born in Kerala, India. He received his BE in electrical engineering from the Gujarat University, India in 2001, his MS in electrical engineering from Iowa State University in 2003 and his Ph.D. in electrical engineering from the University of Wisconsin-Madison in 2008. Currently he is a staff engineer with the Power Electronics Group at United Technologies Research Center. His areas of interest inlcude high density power converter design and analysis.

Damir Zarko was born in Zagreb, Croatia. He received the Dipl. Eng. and M.Sc. degrees in electrical engineering from the University of Zagreb in 1995 and 1999 respectively and the Ph.D. degree from the University of Wisconsin-Madison in 2004. Currently he is an Assistant Professor at the Department of Electrical Machines Drives and Automation, Faculty of Electrical Engineering and Computing, University of Zagreb, Croatia where his research activities are related to design, modelling, analysis and optimization of electrical machines.